

Bayesian Model Calibration and Sensitivity Analysis for Oscillating Biological Experiments

Youngdeok Hwang

Paul H. Chook Department of Information Systems and Statistics
Baruch College, City University of New York

Hang J. Kim, Won Chang

Division of Statistics and Data Science, University of Cincinnati

Christian Hong

Department of Pharmacology and Systems Physiology, University of Cincinnati
and

Steve N. MacEachern

Department of Statistics, The Ohio State University

Abstract

Most organisms exhibit various endogenous oscillating behaviors which provide crucial information as to how the internal biochemical processes are connected and regulated. Understanding the molecular mechanisms behind these oscillators requires interdisciplinary efforts combining both biological and computer experiments, as the latter can complement the former by simulating perturbed conditions with higher resolution. Harmonizing the two types of experiment, however, poses significant statistical challenges due to identifiability issues, numerical instability, and ill behavior in high dimension. This article devises a new Bayesian calibration framework for oscillating biochemical models. The proposed Bayesian model is estimated using an advanced MCMC which can efficiently infer the parameter values that match the simulated and observed oscillatory processes. Also proposed is an approach to sensitivity analysis approach based on the intervention posterior. This approach measures the influence of individual parameters on the target process by utilizing the obtained MCMC samples as a computational tool. The proposed framework is illustrated with circadian oscillations observed in a filamentous fungus, *Neurospora crassa*.

Keywords: Circadian cycle; Differential equation; Generalized multiset sampler; Harmonic basis representation; Intervention posterior; Systematic biology

1 Introduction

Periodicity is one of the common characteristics of biological systems. Organisms demonstrate a diverse range of periodic behaviors regulating distinct molecular, cellular, and physiological phenotypes such as the cell cycle, yeast metabolic cycle, segmentation clock in vertebrates, and circadian rhythms (Tu et al., 2005; Sassone-Corsi et al., 2018). Studying the molecular mechanisms behind these oscillators often requires interdisciplinary efforts combining both physical and computer experiments as computer experiments complement the physical experiments by simulating numerous perturbed conditions at a higher resolution (Sha et al., 2003; Tsai et al., 2008; Gallego et al., 2006; Gotoh et al., 2016).

Computer experiments are widely used to study complex physical processes in various applications such as geoscience (Lee et al., 2020), aerospace engineering (Mak et al., 2018), and biomedical engineering (Sung et al., 2020). Many of these experiments are based on a computer model which consists of a set of differential equations solved by numerical methods. Utilizing these models for further study requires *calibration*, a process to find plausible sets of parameters that produce outcomes similar to those observed in the physical experiment.

Use of the model beyond developing a prototype simulator – for instance for sensitivity analysis or forecasting with model ensembles – is available only after the model is mature and its parameters have been well calibrated. Having a mature model is particularly crucial for counterfactual scenario analyses where the conditions depart from the current steady-state, where a system may become unstable. For example, climate projections under various future CO₂ forcing scenarios require a rigorous quantification and reduction of parametric uncertainty regarding the response of the climate system and heat penetration into the ocean as a prerequisite (e.g., Bellprat et al., 2012; Chang et al., 2014).

Since the seminal work of Kennedy and O’Hagan (2001), computer model calibration has been a major research topic. A particular focus has been on the challenges arising from the high-dimensional, multivariate, and often highly structured outputs that most computer models produce. Bayarri et al. (2007) propose a general statistical framework for computer models with functional outputs. Higdon et al. (2008) introduce a basis representation approach, and Chang et al. (2014) reformulate this approach using dimension reduction to enable faster computing. Gramacy et al. (2015) focus on dealing the large data sets. Chang et al. (2016) and Sung et al. (2020) consider calibration for computer models with binary responses, and Hwang et al. (2018) have incorporated the equations from physics to simplify the calibration framework. There is much interest beyond the statistics community; Karagiannis and Lin (2017), for example, propose a Bayesian approach from the computational physics perspective.

Our work belongs to the broad Bayesian framework of Kennedy and O’Hagan (2001). Despite their overarching perspective and the successful applications that followed (e.g., Higdon et al., 2008), direct application of their framework to our studies faces multiple challenges. First, their formulation presumes that the output is well-behaved so that the input-output relationship can be emulated via a Gaussian process with stationary covariance. When the computer model shows highly nonstationary behavior in certain input spaces, the Gaussian process does not reflect the underlying nature and will lead to poor emulation performance, which will in turn lead to inaccurate calibration. Second, Kennedy and O’Hagan (2001) assume that the physical and computer experiments, as well as their discrepancy, all lie in the same space. Such an assumption allows a direct evaluation of the likelihood in a Bayesian setting, or the objective function in a frequentist setting (e.g., Tuo et al., 2015). In our motivating example, however, the outputs from both physical

and computer experiments are cyclic and oscillating, which requires a customized measure for the discrepancy. A simulator run is deemed successful when it resembles the physical experiment outcome with the curve shifted laterally by some amount, i.e., the computer experiments show peaks that differ from the physical experiments by phase, while the periodicity and magnitude remain approximately the same.

There are three major contributions in our work. First, our modeling approach characterizes the periodicity and amplitude of the oscillating outcome with a harmonic basis representation, so that it captures the cyclical nature of the experiments. Second, we introduce an efficient MCMC approach using the generalized multiset sampler (GMSS, Kim and MacEachern, 2015) to provide a practical solution to evaluate the posterior distribution; the approach is firmly rooted in a rigorous theoretical framework and designed to overcome the challenges of a high-dimensional parameter space and multi-modal posterior densities. Third, we propose an intuitive method for sensitivity analysis, based on the *intervention posterior*, to handle parameter uncertainty. Our framework is illustrated with a case study of physical experiment measurements and a corresponding three-variable, nine parameter computer experiment to study the circadian cycle of a living organism.

The remainder of the paper is organized as follows. Section 2 describes the basic mechanism of oscillating biochemical experiments and the current practice for analysis. Section 3 describes the proposed model and methodology. Section 4 introduces the intervention posterior approach for sensitivity analysis. Section 5 gives an analysis of a three-variable biochemical oscillator using the proposed methodology. We conclude with some remarks and discussion in Section 6.

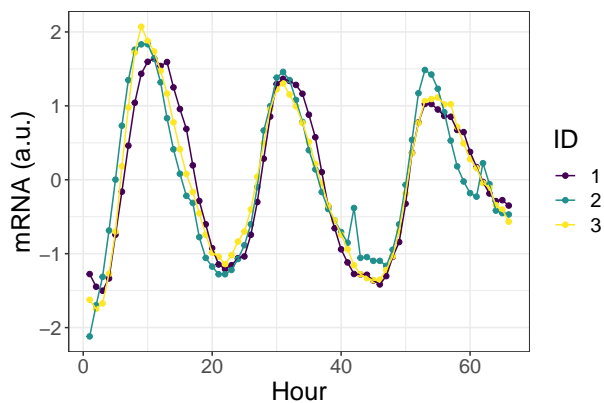


Figure 1: Bioluminescence measurements from a physical experiment with three replicates.

2 Scientific Problem

2.1 Oscillating Biochemical Experiment: Circadian Cycle

Circadian rhythms are events that recur with a period of about 24 hours. The circadian clock governs the periodic behavior that responds to external cues such as the light-dark cycle, and aligns the internal clock to the external environment to optimize an organisms' function and survival. It is known that there exists a conserved molecular mechanism of circadian rhythms in eukaryotes, which consists of transcriptional-translational feedback loops, generating endogenous oscillations of about 24 hours (Dunlap and Loros, 2017; Cox and Takahashi, 2019). Misalignment of the internal circadian clock and the external environment increases the risk of sleep disorders, as well as cardiovascular and metabolic diseases. Thus, it is critical to understand the fundamental molecular mechanisms of the circadian rhythms and their signaling pathways to other mechanisms such as the cell cycle or metabolism.

In this work, we use the circadian cycle of a filamentous fungus *Neurospora crassa*. *Neurospora crassa* has been a model organism for understanding circadian clocks since the 1950s, when its physiological output became tractable to biologists (Dunlap and Loros,

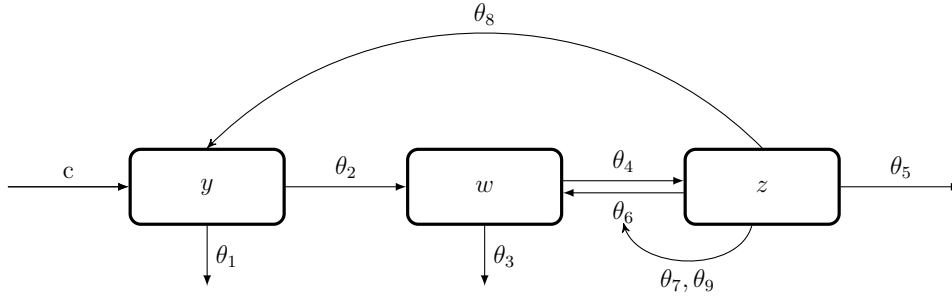


Figure 2: The schematic illustration of the oscillator experiment.

2017). Physical experiments in this study produce indirect measurements of the gene expression activity of the gene named *frequency* (*frq*), which is known to regulate the circadian cycle of *Neurospora crassa*. The activity of *frq* gene expression is measured using bioluminescence assays detecting the activity of luciferase driven by the *frq* promoter (Gooch et al., 2014). Bioluminescence is detected by a software-controlled camera collecting the measurements for 10 minutes every hour. Figure 1 depicts the three replicates from physical experiments we use in this study, where we observe endogenous cycles of approximately 21-22 hours.

As a counterpart of the physical experiments, we consider a mathematical model of the molecular mechanisms of oscillators regulated by nonlinear dynamics defined by a set of ordinary differential equations (ODE) from Caicedo-Casso et al. (2015). This model reflects recently discovered self-regulatory negative- and positive-feedback loops (Aronson et al., 1994; Liu et al., 2019). It consists of three state variables: *frq* mRNA (y), protein (w), and phosphorylated protein (z) as their main variables, where the system wiring is characterized by nine unknown parameters $\boldsymbol{\theta} = (\theta_1, \dots, \theta_9)$ that are related to biological processes, such as the synthesis rate or the threshold of critical concentration. The parameter related to the rate of transcription of y is fixed at c . Caicedo-Casso et al. (2015) wrote the dynamical

system as

$$\frac{dy}{dt} = \frac{c}{1 + (z/\theta_8)^8} - \theta_1 y, \quad (1)$$

$$\frac{dw}{dt} = \theta_2 y - (\theta_3 + \theta_4)w + \theta_6 z - \frac{\theta_7 w z^4}{\theta_9^4 + z^4}, \quad (2)$$

$$\frac{dz}{dt} = \theta_4 w - (\theta_5 + \theta_6)z + \frac{\theta_7 w z^4}{\theta_9^2 + z^4}. \quad (3)$$

In this system, the *frq* mRNA (y) is translated into protein (w), and this protein is transformed into the end product (z). Figure 2 presents a schematic illustration of this system, where arrows represent how each process is involved in the process. For example, θ_1 in (1) is the degradation rate for y , and θ_2 in (2) the rate of translation from y to w . From Figure 2 and equations (1)-(3), it can be seen that the system has self-regulating feedback loops; for example, a high level of y leads to a higher level of w through θ_2 , then higher z through θ_4 , but the increase in z (modulated by θ_8) hinders the transcription of y . The amount of mRNA in the computer experiment, y , is to be matched with the bioluminescence measurements from physical experiments for model calibration.

2.2 Current Practices in Mathematical Biology

When studying a phenomenon using both computer and physical experiments, it is imperative to harmonize the two sources by tuning the parameters of the computer model to match physical measurements. Although oscillating biological systems have been studied for decades, a framework for the coherent analysis and parameter estimation of those models has not yet been established. Typical analyses begin with an initial parameter value adopted from the existing literature, or derived from an experimenter's hunch. From this value, a search for a *better* parameter value proceeds, perhaps by trial-and-error or with a

more formal yet heuristic search algorithm. The search terminates when a *reasonable* value θ_0 is found or when a convergence criterion is satisfied. This search may or may not be directly tied to the data from the physical experiment. One tradition relies on a subjective match of qualitative features of the computer model outputs and physical experiment measurements, often based on a visual examination. Another batch of typical estimation strategies is to use optimization algorithms, such as simulated annealing (Kirkpatrick, 1984; Bellman et al., 2018), differential evolution (Storn and Price, 1997; Oguz et al., 2013), or multiple shooting (Peifer and Timmer, 2007) to name a few. These optimization-based approaches are often limited by slow convergence and local traps, while being overly sensitive to tuning parameters such as temperature in simulated annealing or differential weights in differential evolution. They also lack a suitable measure of uncertainty; the limitations are often not clearly addressed in the biological sciences or applied mathematics literature (e.g., Bellman et al., 2018).

It is common to conduct a sensitivity analysis once θ_0 is settled. The sensitivity analysis mainly seeks to understand qualitative changes in the system behavior, or numerical changes in a target quantity as the parameters deviate from θ_0 (Goodfellow et al., 2014; Caicedo-Casso et al., 2015; Liu et al., 2019). However, such an approach fails to incorporate the inherent uncertainty in estimating the model parameters θ . A detailed discussion on how to address this issue statistically follows in the next section.

3 Bayesian Model Formulation and Posterior Inference for the Oscillating Biochemical Experiment

Many parameters in computer experiments are unknown to the experimenters, and the computer experiments often cannot fully reflect reality, causing some degree of bias. Since the seminal work of Kennedy and O’Hagan (2001), Bayesian approaches have been widely used for computer model calibration, and inference problems have been cast in the Kennedy-O’Hagan framework. In this section, we present our modeling approach to integrate the physical and computer experiments based on Bayesian inference.

3.1 Bayesian Hierarchical Model with Harmonic Basis Representation

Let $\mathbf{y}_i^F = (y_{i1}^F, \dots, y_{iT}^F)^\top$ denote the measurements obtained from the i th physical experiment. To incorporate the strong periodicity of the observed data, we formulate

$$y_{it}^F = \sum_{k=1}^K a_{ik} \cos\left(\frac{2\pi kt}{T}\right) + \sum_{k=1}^K b_{ik} \sin\left(\frac{2\pi kt}{T}\right) + \varepsilon_{it}^F, \quad (4)$$

for $i = 1, \dots, n$ and $t = 0, \dots, T - 1$, where ε_{it}^F is assumed to be an independent error from $N(0, \sigma_F^2)$. To characterize the overall amplitude of data from a physical experiment, we consider $s_{ik} = a_{ik}^2 + b_{ik}^2$, the power spectrum of the k th frequency component, which represents the magnitude of periodic behavior at the frequency of k/T in the i th observed time series (Hartley, 1949). For example, the data sets presented in Figure 1 have $T = 66$, so s_{i1} represents the magnitude of the periodic behavior that completes its cycle once every 66 hours, s_{i2} every 33 hours, and so on. Applying the basic properties of trigonometric functions, it can be shown that the design matrix for (4) is orthogonal and results in the least square

estimates, $\hat{a}_{ik} = (2/T) \sum_{t=0}^{T-1} y_{it}^F \cos(2\pi kt/T)$ and $\hat{b}_{ik} = (2/T) \sum_{t=0}^{T-1} y_{it}^F \sin(2\pi kt/T)$. Let $\hat{s}_{ik} = \hat{a}_{ik}^2 + \hat{b}_{ik}^2$. Then under the normality assumption in (4), we have $\hat{s}_{ik}|s_{ik} \sim \chi_2^2(V_{ik}^{-1}s_{ik})$, $k = 1, \dots, K$, where $V_{ik} = \sigma^2 \sum_{t=0}^{T-1} \{\cos(2\pi kt/T)\}^2 = \sigma^2 \sum_{t=0}^{T-1} \{\sin(2\pi kt/T)\}^2 = T\sigma^2/2$. The estimated power spectrum \hat{s}_{ik} represents the variance component of \mathbf{y}_i^F attributable to the k th frequency (Geoghegan, 2006).

For the computer experiments, let $\mathbf{y}^M(\boldsymbol{\theta}) = (y_1^M(\boldsymbol{\theta}), \dots, y_T^M(\boldsymbol{\theta}))^\top$ denote outcomes from a computer model, or a *mathematical* model, executed with the input parameters $\boldsymbol{\theta} = (\theta_1, \dots, \theta_p)$. Then, we express the computer model outcomes by

$$y_t^M(\boldsymbol{\theta}) = \sum_{k=1}^K \alpha_k(\boldsymbol{\theta}) \cos\left(\frac{2\pi kt}{T}\right) + \sum_{k=1}^K \beta_k(\boldsymbol{\theta}) \sin\left(\frac{2\pi kt}{T}\right) + \varepsilon_t^M, \quad (5)$$

for $t = 0, \dots, T-1$, where $\varepsilon_t^M \stackrel{iid}{\sim} N(0, \sigma_M^2)$. We define $\lambda_k(\boldsymbol{\theta}) \equiv \alpha_k^2(\boldsymbol{\theta}) + \beta_k^2(\boldsymbol{\theta})$ for the model outputs, similarly to s_{ik} from the field data.

The formulations in (4) and (5) are basis representations based on harmonic basis functions. A suite of different basis functions has been employed in the computer experiments literature, including wavelets (Bayarri et al., 2007), principal components (Higdon et al., 2008; Chang et al., 2014, 2016), Gaussian kernels (Bhat et al., 2012), and spherical harmonics (Chang and Guillas, 2019). To the best of our knowledge, however, harmonics has not been used to characterize the periodic behavior in computer model calibration literature. Chang and Guillas (2019) used spatial harmonics to facilitate computation by reducing the rank of the spatial covariance matrix to avoid prohibitive matrix computation in the likelihood evaluation, not to model the cyclical behavior using the basis representation.

Our modeling approach is in the spirit of the spectral analysis, yet our focus is on the cyclical behavior at lower frequencies, obtained from the limited physical experiments. Following the Kennedy-O'Hagan framework, we connect the outputs of the physical exper-

iment and the computer model using the underlying spectrum by $s_{ik} = \lambda_k(\boldsymbol{\theta}) + \delta_{ik}$ with the computer model discrepancy $\delta_{ik} \sim N(0, \tau^2)$ for $i = 1, \dots, n$ and $k = 1, \dots, K$. To conclude the hierarchical structure for calibration, adding prior distributions for λ_k and τ^2 gives the following hierarchical Bayesian model

$$\hat{s}_{ik}|s_{ik} \sim \chi_2^2(V_{ik}^{-1}s_{ik}), \quad s_{ik}|\lambda_k, \tau^2 \sim N^+(\lambda_k, \tau^2), \quad \theta_j \sim \text{IG}(a_\theta, b_\theta), \quad \tau^2 \sim \text{IG}(a_\tau, b_\tau) \quad (6)$$

for $i = 1, \dots, n$, $j = 1, \dots, p$ and $t = 0, \dots, T - 1$ given the data \hat{s}_{ik} , where N^+ and IG denote the truncated normal distribution above zero and the inverse gamma distribution, respectively.

The likelihood functions directly contain the model spectrum $\lambda_k = \lambda_k(\boldsymbol{\theta})$, so the computer experiment needs to be evaluated for each MCMC iterate. Our approach is most suitable when the computer experiments are computationally affordable (e.g., Williams et al., 2011; Lee et al., 2020) as in the setting described in Section 2. It still remains to design an MCMC that can obtain a set of usable posterior samples for adequate uncertainty quantification of the irregular densities that arise from the nonlinear mathematical model. We address these difficulties in the following section.

3.2 Posterior Estimation by the Generalized Multiset Sampler

The oscillating computer model given in (1) - (3) only produces a solution in a small portion of the entire model parameter space. Moreover, the solution region often consists of many narrow sub-regions that are disconnected from each other, while scattered around the high-dimensional parameter space. Parameters regulating the oscillatory process have complex interactions between them, where a small change in a parameter may make one particular stimulus dominate the entire feedback loop process, rendering the regulating cycle inoperative. Consequently, the likelihood function is very low in the majority of the

input space, as the computer model produces a circadian cycle with little to no variation of mRNA level therein. This situation poses a critical challenge for a standard MCMC algorithm. Although the Markov chain converge to the posterior distribution in theory, the presence of multiple local maxima and the narrow high-likelihood regions cause the sampler to get trapped in a local mode or to show prohibitively slow convergence and mixing.

Such issues have long been recognized as a major challenge in applications of MCMC sampling. A large class of advanced Monte Carlo algorithms has been proposed to alleviate this issue. Examples include the tempering algorithm and its variants (Swendsen and Wang, 1986; Geyer, 1991; Marinari and Parisi, 1992), the multiple-try Metropolis algorithm (Liu et al., 2000), and the multiset sampler (Leman et al., 2009; Kim and MacEachern, 2015).

The conditional distribution of all unknown parameters in the hierarchical Bayesian model (6) is $f(\boldsymbol{\theta}, \mathbf{S}, \tau^2 | \widehat{\mathbf{S}}) \propto \left[\prod_{i=1}^n \prod_{k=1}^K f(\hat{s}_{ik} | s_{ik}) f(s_{ik} | \lambda_k(\boldsymbol{\theta}), \tau^2) \right] f(\boldsymbol{\theta}) f(\tau^2)$ where $\mathbf{S} = \{s_{ik} : i = 1, \dots, n, k = 1, \dots, K\}$ and $\widehat{\mathbf{S}} = \{\hat{s}_{ik} : i = 1, \dots, n, k = 1, \dots, K\}$. A standard posterior inference approach using the Metropolis-within-Gibbs is given in the Appendix with detailed steps. We confirmed that the standard MCMC fails to explore the entire posterior distribution due to severe multimodality in a high-dimensional space. We address these challenges by using an advanced MCMC method called the generalized multiset sampler.

The multiset sampler (Leman et al., 2009) is an MCMC algorithm originally designed to make inference for a multimodal distribution. Suppose that \mathbf{y} is a set of observations and $\boldsymbol{\theta} \in \Omega$ is a vector of parameters whose posterior density is expected to be multimodal. The central idea of the multiset sampler is to define a multiset $\Theta = \{\boldsymbol{\theta}_1, \dots, \boldsymbol{\theta}_M\}$, draw MCMC samples of the multiset, and make inference about $\boldsymbol{\theta}$ by statistically fusing the multiple copies of $\boldsymbol{\theta}_m$ in the multiset, instead of directly sampling the original parameter $\boldsymbol{\theta}$. When

the target posterior density is $f(\boldsymbol{\theta}|\mathbf{y})$, the multiset sampler updates the parameters with its multiset *sampling* distribution $\pi(\boldsymbol{\Theta}|\mathbf{y})$, defined as $\pi(\boldsymbol{\Theta}|\mathbf{y}) \propto \sum_{m=1}^M f(\boldsymbol{\theta}_m|\mathbf{y})$. For the m th multiset element at iteration $b = 1, \dots, B$, the MCMC updates $\boldsymbol{\theta}_m$ via the Metropolis-Hastings algorithm: propose $\boldsymbol{\theta}_m^q \sim q(\boldsymbol{\theta}_m^q|\boldsymbol{\theta}_m^{(b-1)})$ and accept as $\boldsymbol{\theta}_m^{(b)} = \boldsymbol{\theta}_m^q$ with the acceptance probability $\min\{1, \alpha_m^{(b)}\}$, where

$$\alpha_m^{(b)} = \frac{f(\boldsymbol{\theta}_m^q|\mathbf{y}) + \sum_{l \neq m} f(\boldsymbol{\theta}_l^{(b-1)}|\mathbf{y})}{f(\boldsymbol{\theta}_m^{(b-1)}|\mathbf{y}) + \sum_{l \neq m} f(\boldsymbol{\theta}_l^{(b-1)}|\mathbf{y})} \frac{q(\boldsymbol{\theta}_m^{(b-1)}|\boldsymbol{\theta}_m^q)}{q(\boldsymbol{\theta}_m^q|\boldsymbol{\theta}_m^{(b-1)})}.$$

This accept-reject update shows how the multiset sampler avoids getting stuck in a local mode. For the simplicity of illustration, let us assume that the proposal distribution is symmetric, so that $q(\boldsymbol{\theta}_m^{(b-1)}|\boldsymbol{\theta}_m^q)/q(\boldsymbol{\theta}_m^q|\boldsymbol{\theta}_m^{(b-1)})$ is always one, although this is not necessary in practice. If $\boldsymbol{\theta}_m^{(b-1)}$ is associated with a large value of $f(\boldsymbol{\theta}_m^{(b-1)}|\mathbf{y})$, the value of α is close to $f(\boldsymbol{\theta}_m^q|\mathbf{y})/f(\boldsymbol{\theta}_m^{(b-1)}|\mathbf{y})$, so it behaves similarly to a standard random walk Metropolis-Hastings exploring the original target distribution $f(\boldsymbol{\theta}|\mathbf{y})$. This multiset element is called the *leading* element. Meanwhile, if $\boldsymbol{\theta}_m^{(b-1)}$ is associated with a relatively small value of $f(\boldsymbol{\theta}_m^{(b-1)}|\mathbf{y})$, it contributes little to $f(\boldsymbol{\theta}_m^{(b-1)}|\mathbf{y}) + \sum_{l \neq m} f(\boldsymbol{\theta}_l^{(b-1)}|\mathbf{y})$ and hence the acceptance probability for the proposed $\boldsymbol{\theta}_m^q$ becomes nearly one no matter what value is suggested for $\boldsymbol{\theta}_m^q$. This element of the multiset sampler is let loose in Ω , avoiding getting stuck in a local mode, and is called a *non-leading* multiset element.

The generalized multiset sampler (GMSS, Kim and MacEachern, 2015) further refines the idea of multiset sampler, by explicitly linking the sampling distribution to the target distribution and utilizing an auxiliary density to guide the movement of the Markov chain to plausible areas. Specifically, it defines the multiset sampling distribution by

$$\pi(\boldsymbol{\Theta}|\mathbf{y}) = \frac{1}{M} \sum_{m=1}^M f(\boldsymbol{\theta}_m|\mathbf{y}) \prod_{l \neq m} g_l(\boldsymbol{\theta}_l), \quad (7)$$

where g_l is an instrumental density with the same support as $\boldsymbol{\theta}$, then provides estimation strategies for any density of interest, using importance sampling. In this general framework, the original multiset sampler of Leman et al. (2009) can be considered as a special case of (7) where $g_l(\boldsymbol{\theta}_l)$ is set to be a uniform distribution on a bounded support.

With some algebra, the marginal sampling density of each multiset element is easily derived from (7) as $\pi(\boldsymbol{\theta}_m|\mathbf{y}) = (1/M)f(\boldsymbol{\theta}_m|\mathbf{y}) + \{1 - (1/M)\}g_m(\boldsymbol{\theta}_m)$ for $m = 1, \dots, M$, which is a weighted sum of the target density $f(\boldsymbol{\theta}|\mathbf{y})$ and the instrumental density $g_m(\boldsymbol{\theta})$. Similar to the role of the instrumental density in the importance sampling, the GMSS instrumental density g_m is a tuning density that gently herds the sampler toward a promising area. If $g_m(\boldsymbol{\theta})$ is precisely chosen to be $f(\boldsymbol{\theta}_m|\mathbf{y})$, the marginal sampling distribution $\pi(\boldsymbol{\theta}_m|\mathbf{y})$ becomes the target distribution $f(\boldsymbol{\theta}|\mathbf{y})$ which guarantees the most efficient sampling scheme; yet even crude information on the target density is useful to form an instrumental density in practice. For any integrable function of the parameters, $h(\boldsymbol{\theta})$, the final inference on $h(\boldsymbol{\theta})$ under the target posterior $f(\boldsymbol{\theta}|\mathbf{y})$ is made from the GMSS sampling distribution $\pi(\boldsymbol{\Theta}|\mathbf{y})$ by Theorem 1 in Kim and MacEachern (2015), which is restated below:

Theorem 1. Define a set of weights

$$w_m = \frac{f(\boldsymbol{\theta}_m|\mathbf{y}) \prod_{l \neq m} g_l(\boldsymbol{\theta}_l)}{\sum_{m'=1}^M f(\boldsymbol{\theta}_{m'}|\mathbf{y}) \prod_{l' \neq m'} g_{l'}(\boldsymbol{\theta}_{l'})} \quad \text{for } m = 1, \dots, M.$$

Then, for any integrable function h , $E_f \{h(\boldsymbol{\theta})|\mathbf{y}\} = E_\pi \left\{ \sum_{m=1}^M w_m h(\boldsymbol{\theta}_m) \middle| \mathbf{y} \right\}$.

This theorem implies that the importance of elements in each multiset is reflected in the final inference via weight w_m .

The conditional density under the GMSS sampling distribution π is found by the following Metropolis-within-Gibbs steps. For each MCMC iteration $b = 1, \dots, B$, and for component $m = 1, \dots, M$, propose $\boldsymbol{\theta}_m^a \sim q(\boldsymbol{\theta}_m^a|\boldsymbol{\theta}_m^{(b-1)})$ and let $\boldsymbol{\theta}_m^{(b)} = \boldsymbol{\theta}_m^a$ with proba-

bility $\min(1, \alpha_m^{(b)})$ where $\alpha_m^{(b)} = \{\pi(\Theta_m^q | \mathbf{y}) / \pi(\Theta_m^{(b-1)} | \mathbf{y})\} \{q(\theta_m^{(b-1)} | \theta_m^q) / q(\theta_m^q | \theta_m^{(b-1)})\}$ with the proposed multiset $\Theta_m^q = \{\theta_1^{(b)}, \dots, \theta_{m-1}^{(b)}, \theta_m^q, \theta_{m+1}^{(b-1)}, \dots, \theta_M^{(b-1)}\}$ and the current state $\Theta_m^{(b-1)} = \{\theta_1^{(b-1)}, \dots, \theta_{m-1}^{(b-1)}, \theta_m^{(b-1)}, \dots, \theta_M^{(b-1)}\}$. Then, the formal estimator of any target posterior quantity for a function $h(\theta)$, $E_f\{h(\theta) | \mathbf{y}\}$, is computed with the GMSS samples by

$$\widehat{E}_f\{h(\theta) | \mathbf{y}\} = \frac{1}{B} \sum_{b=1}^B \sum_{m=1}^M w_m^{(b)} h(\theta_m^{(b)}). \quad (8)$$

where the set of weights at the b th iteration is calculated as

$$w_m^{(b)} = \{f(\theta_m^{(b)} | \mathbf{y}) \prod_{l \neq m} g_l(\theta_l^{(b)})\} / \{M \pi(\Theta^{(b)} | \mathbf{y})\} \text{ where } \Theta^{(b)} = \{\theta_1^{(b)}, \dots, \theta_M^{(b)}\}.$$

Using the instrumental densities, the GMSS makes an explicit link between the target distribution $f(\theta | \mathbf{y})$ and the sampling distribution $\pi(\Theta | \mathbf{y})$ used in the MCMC. The generalized formulation allows the algorithm to be run on unbounded parameter space Ω and improves estimation. Moreover, a well chosen set of instrumental densities $\{g_m(\theta_m) : m = 1, \dots, M\}$ increases the efficiency of the sampler when target posterior density is narrow and multimodal or the parameter space is high dimensional. For example, Kim and MacEachern (2015) showed that the GMSS performs well in the example with a mixture of 10-dimensional normal distributions, which is both multimodal and high dimensional. We find the instrumental densities using a large prognostic experiment with distributed computing, as described in the following subsection.

3.3 Finding Instrumental Densities of the GMSS Using Prognostic Experiments

The flexibility of GMSS with instrumental densities $g_m(\theta_m)$ provides an opportunity to improve the MCMC. Well chosen instrumental densities, that are approximately proportional to the unknown target posterior densities and positive in the support of the target posterior

densities, can drastically accelerate the MCMC convergence by sampling more frequently from more promising input spaces. To find such a small target area, our approach evaluates the likelihood function with numerous input parameter settings using parallelized high-throughput computing systems with many cores *prior* to initiating the MCMC computation. With those evaluations, the input space is categorized into two groups: areas with prospects that appear more likely and less likely, respectively.

Without loss of generality, we assume that the univariate parameter space is $(0, 1]$ for each dimension of the parameter $\boldsymbol{\theta}$ after appropriate scaling and transformation. We first create a large design \mathcal{D} of N runs, $\boldsymbol{\theta}_1, \dots, \boldsymbol{\theta}_N$, where each run is independently generated from $U(0, 1]^p$, and conduct experiments on them to obtain $(\boldsymbol{\theta}_1, \mathbf{y}_1), \dots, (\boldsymbol{\theta}_N, \mathbf{y}_N)$, where \mathbf{y}_k is the output associated with $\boldsymbol{\theta}_k$. Since each run is independently generated, they can be readily distributed over multiple machines. To define the instrumental density, we adopt an approach inspired by the orthogonal array-based space-filling design (OASD, Tang, 1993). The OASD was originally developed to achieve variance reduction in mean estimates when a small number of computer experiments can be afforded. Our focus is, however, systematically indexing the input space using the orthogonal array structure while effectively utilizing the computational resources.

Let $\lceil \cdot \rceil$ denote the ceiling function. We divide $(0, 1]$ into q partitions of equal lengths, $(0, 1/q], (1/q, 2/q], \dots, ((q-1)/q, 1]$, and define $u_q(\theta) = \lceil \theta q \rceil, \theta \in (0, 1]$, which maps the parameters from $(0, 1]$ to $\{1, \dots, q\}$. Similarly define $u_q(\boldsymbol{\theta}) = (u_q(\theta_1), \dots, u_q(\theta_p))$ with the element-wise mapping. With this mapping, any point in $(0, 1]^p$ is associated with a level combination in a q^p factorial design. We examine the outcomes of \mathcal{D} mapped on the factorial design space. Let $\mathcal{S} = \{1, \dots, p\}$ and consider all possible subsets $\mathcal{S}_b \subset \mathcal{S}$ with $|\mathcal{S}_b| = d_0 \leq p$ for $b = 1, \dots, \binom{p}{d_0}$, where d_0 is the chosen subspace search size specified by the user. This

choice of d_0 leads to a q^{d_0} factorial design for each \mathcal{S}_b . Let $\mathcal{H}_b = \{h_b^{(1)}, \dots, h_b^{(q^{d_0})}\}$ denote the level combinations corresponding to \mathcal{S}_b , and $\omega_{\mathcal{S}_b}$ the level combination associated with ω in \mathcal{S}_b for a $\omega \in (0, 1]^p$.

Now choose a l_{\min} and n_{\min} , where the former is the minimum threshold for the evaluated likelihood in (6) denoted by $l(\boldsymbol{\theta})$ below, and the latter the minimum number of successful runs for a design space to be considered as a high prospect area. With chosen l_{\min} , find $G_b(h) = \{\omega \in \mathcal{D} : u_q(\omega_{\mathcal{S}_b}) = h, l(\boldsymbol{\theta}) > l_{\min}\}$ for $b = 1, \dots, \binom{p}{d_0}$ and $h \in \mathcal{H}_b$. If $|G_b(h)| > n_{\min}$, the search categorizes $\{\omega \in (0, 1]^p : u_q(\omega_{\mathcal{S}_b}) = h\}$ as a high prospect area. Note that each element in \mathcal{H}_b represents q^{-d_0} fraction of $(0, 1]^p$ space, yet \mathcal{S}_b and $\mathcal{S}_{b'}$ with $b \neq b'$ consider a projection into different subspaces.

After the search process, we set the instrumental density as $g_m(\omega) = \rho_1$ for the high prospect area and ρ_0 for the low prospect area, for all m . The values of ρ_0 and ρ_1 are determined by the analyst to reflect the relative importance of the two areas in guiding the multiset sampler. They need to be scaled appropriately so that $g_m(\omega)$ is a legitimate density function, i.e., $\int_{\Omega} g_m(\omega) d\boldsymbol{\theta} = 1$. An area in $(0, 1]^q$ receives a higher weight if it has more than n_{\min} successful runs in any of its d_0 dimensional projections from prognostic experiments. This difference in instrumental densities gently guides non-leading multiset elements more likely exploring the high *prospect* area, while the leading multiset element stays around the currently known high *density* region.

The instrumental densities obtained using the high prospect area can be viewed as a simple form of density estimation where the algorithm parameters q and d_0 determine the computational complexity. These parameters can be interactively chosen while analyzing the results from prognostic experiments, where some practical consideration can be employed: the amount of available computation resources, the number of dimensions, and the

behavior of the computer experiments. In general, one can apply empirical principles of factorial effects, hierarchy, sparsity and heredity (Wu and Hamada, 2011). For example, choosing $d_0 = p$ is equivalent to examining every level combination in q^p factorial design and gives ρ_1 to each q^{-p} fraction with more than n_{\min} runs with the likelihood higher than l_{\min} , yet it requires a large N to have enough evaluation for each level combination. In our case study, $p = 9$ and $d_0 = 4$, so that every evaluation uses 3^5 times more runs. Using a $d_0 < p$ allows a faster search on q^{d_0} compared to q^p , similar to the benefit of using fractional factorial designs over full factorial designs.

3.4 MCMC Steps with the GMSS

With the hierarchical Bayesian model (6), the joint posterior distribution of the multiset $\Theta = (\theta_1, \dots, \theta_M)$ and other model parameters is written by

$$\begin{aligned} \pi(\Theta, \mathbf{S}, \tau^2 | \widehat{\mathbf{S}}) &= \frac{1}{M} \sum_{m=1}^M f(\theta_m, \mathbf{S}, \tau^2 | \widehat{\mathbf{S}}) \prod_{l \neq m} g_l(\theta_l) \\ &\propto \left\{ \prod_{i=1}^n \prod_{k=1}^K f(\widehat{s}_{ik} | s_{ik}) \right\} f(\tau^2) \left[\frac{1}{M} \sum_{m=1}^M \left\{ \prod_{i=1}^n \prod_{k=1}^K f(s_{ik} | \lambda_k(\theta_m), \tau^2) \right\} f(\theta_m) \prod_{l \neq m} g_l(\theta_l) \right]. \end{aligned}$$

Then, the estimation of $f(\Theta, \mathbf{S}, \tau^2 | \widehat{\mathbf{S}})$ is based on the following MCMC steps.

1. Update the ODE model parameter $\theta_{m,j}$ for each $m = 1, \dots, M$ and $j = 1, \dots, p$.

Propose $\theta_{m,j}^q$ from the normal distribution with mean $\theta_{m,j}$ and a standard deviation set by the analyst as a step size. Set $\theta_m^q = (\theta_{m,1}, \dots, \theta_{m,j-1}, \theta_{m,j}^q, \theta_{m,j+1}, \dots, \theta_{m,p})$.

For all $l \neq m$, $\theta_l^q = (\theta_{l,1}, \dots, \theta_{l,p})$. Then, update $\theta_{m,j} = \theta_{m,j}^q$ with the acceptance probability, $\min(1, a)$, where

$$a = \frac{\sum_{m'=1}^M \left\{ \prod_{i=1}^n \prod_{k=1}^K f(s_{ik} | \lambda_k(\theta_{m'}^q), \tau^2) \right\} f(\theta_{m'}^q) \prod_{l \neq m'} g_l(\theta_l^q)}{\sum_{m'=1}^M \left\{ \prod_{i=1}^n \prod_{k=1}^K f(s_{ik} | \lambda_k(\theta_{m'}), \tau^2) \right\} f(\theta_{m'}) \prod_{l \neq m'} g_l(\theta_l)}$$

and $\lambda_k(\boldsymbol{\theta})$ is k -th amplitude computed from the spectral analysis given the ODE parameters $\boldsymbol{\theta}$.

2. Update $\mathbf{s}_i = (s_{i1}, \dots, s_{iK})$ for each $i = 1, \dots, n$. Propose $\mathbf{s}_i^q = (s_{i1}^q, \dots, s_{iK}^q)$ by proposing $s_{i'k}^q$ from the normal distribution with mean $s_{i'k}$ and a standard deviation set by the analyst as a step size for $k = 1, \dots, K$. For $i' \neq i$, let $\mathbf{s}_{i'}^q = (s_{i'1}, \dots, s_{i'K})$.

Then, update $\mathbf{s}_i = \mathbf{s}_i^q$ with the acceptance probability, $\min(1, a)$, where

$$a = \frac{\prod_{k=1}^K f(\hat{s}_{ik} | s_{ik}^q) \left[\sum_{m=1}^M \left\{ \prod_{i'=1}^n \prod_{k=1}^K f(s_{i'k}^q | \lambda_k(\boldsymbol{\theta}_m), \tau^2) \right\} f(\boldsymbol{\theta}_m) \prod_{l \neq m} g_l(\boldsymbol{\theta}_l) \right]}{\prod_{k=1}^K f(\hat{s}_{ik} | s_{ik}) \left[\sum_{m=1}^M \left\{ \prod_{i'=1}^n \prod_{k=1}^K f(s_{i'k} | \lambda_k(\boldsymbol{\theta}_m), \tau^2) \right\} f(\boldsymbol{\theta}_m) \prod_{l \neq m} g_l(\boldsymbol{\theta}_l) \right]}.$$

3. Update τ^2 by the Metropolis-Hastings. Propose τ^{2q} from the normal distribution with mean τ^2 and a standard deviation set by the analyst. Then, update $\tau^2 = \tau^{2q}$ with the acceptance probability, $\min(1, a)$, where

$$a = \frac{\sum_{m=1}^M \left\{ \prod_{i=1}^n \prod_{k=1}^K f(s_{ik} | \lambda_k(\boldsymbol{\theta}_m), \tau^{2q}) \right\} f(\boldsymbol{\theta}_m) \prod_{l \neq m} g_l(\boldsymbol{\theta}_l) f(\tau^{2q})}{\sum_{m=1}^M \left\{ \prod_{i=1}^n \prod_{k=1}^K f(s_{ik} | \lambda_k(\boldsymbol{\theta}_m), \tau^2) \right\} f(\boldsymbol{\theta}_m) \prod_{l \neq m} g_l(\boldsymbol{\theta}_l) f(\tau^2)}.$$

4 Sensitivity Analysis via Intervention Posterior

Computer experiments have the goal of providing insight into a system, often by identifying the key factors that drive the system's behavior. In our setting, we have access to limited physical experimental data, i.e., the bioluminescence data, that have been collected under a single condition. We can combine the limited experimental data with a wealth of data from the computer experiment, providing $\mathbf{y}^M(\boldsymbol{\theta})$. The posterior distribution arises from combination of the prior distribution over $\boldsymbol{\theta}$, hence implicitly over $\mathbf{y}^M(\boldsymbol{\theta})$, and the data from the physical experiment, \mathbf{y}_i^F for $i = 1, 2, 3$. Our task is to provide guidance to the biologists as to what changes to the system are likely to result in substantive changes to

its specified features which are of researchers' analytical interest.

The computer model is built on $\boldsymbol{\theta}$, a vector of parameters in the ODE, that relate to biochemical processes. Experimentally, the biologists hope to discover interventions that directly affect one of these processes, thereby affecting the behavior of the system. The central question here is which experimental configuration is to be manipulated to move the specified feature of the manipulated system toward a target value. Their question follows a chain of causality – experimental manipulation, or *intervention*, to change biochemical processes captured by parameters in the ODE with the goal of impacting a selected feature given by $h(\boldsymbol{\theta})$, a function of the parameters of research interest.

For a system with known parameters, the sensitivity of $h(\boldsymbol{\theta})$ to a change in a single parameter, say θ_j , would be captured by defining

$$\boldsymbol{\nu}_{j,\alpha} = \boldsymbol{\nu}_{j,\alpha}(\boldsymbol{\theta}) = (\theta_1, \dots, \theta_{j-1}, \alpha\theta_j, \theta_{j+1}, \dots, \theta_p), \quad (9)$$

and then computing $h(\boldsymbol{\nu}_{j,\alpha})$ for a range of values of a scale parameter, α . All perturbations under consideration must result in perturbed parameter values that lie within the parameter space. Alternatively, one could consider the local sensitivity of the feature with respect to an infinitesimal perturbation of θ_j via $\partial h(\boldsymbol{\theta})/\partial\theta_j$. Sensitivity to changes in a collection of parameters can be handled in analogous fashion.

As in most of the calibration problem, we do not know the true value of $\boldsymbol{\theta}$ for the single condition where we have data from physical experimentation. Rather, our knowledge of the parameter under the experimental treatment is captured in the posterior distribution $f(\boldsymbol{\theta}|\mathbf{y})$. We seek the related distribution for the parameters if the biologist were to intervene with an experimental manipulation, which alters some parameters in $\boldsymbol{\theta}$. We call this distribution the *intervention posterior*, $f_I(\boldsymbol{\theta}|\mathbf{y})$. Partitioning the parameter vector $\boldsymbol{\theta}$ into two parts, $\boldsymbol{\theta} = (\boldsymbol{\eta}, \boldsymbol{\xi})$, we write the posterior density as $f(\boldsymbol{\theta}|\mathbf{y}) = f_{\boldsymbol{\eta}}(\boldsymbol{\eta}|\mathbf{y}) \cdot f_{\boldsymbol{\xi}}(\boldsymbol{\xi}|\boldsymbol{\eta}, \mathbf{y})$. Par-

alleling the situation where the system parameters are known, we consider a scale change for ξ , which gives $f_I(\boldsymbol{\theta}|\mathbf{y}) = f_\eta(\boldsymbol{\eta}|\mathbf{y}) \cdot f_{I,\xi}(\xi|\boldsymbol{\eta}, \mathbf{y})$. For example, in the event that $\xi = \theta_j$, a scale change on θ_j by α would take $\boldsymbol{\theta}$ to $\boldsymbol{\nu}_{j,\alpha}$ in (9), leaving the part corresponding to $\boldsymbol{\eta}$ unchanged.

The intervention posterior gives us access to the distribution induced on $h(\boldsymbol{\nu}_{j,\alpha})$ by manipulation of the experimental conditions to impact $\boldsymbol{\theta}$. It can be seen from the expression of the intervention posterior mean,

$$\int h(\boldsymbol{\nu}_{j,\alpha}(\boldsymbol{\theta}))f(\boldsymbol{\nu}_{j,\alpha}(\boldsymbol{\theta})|\text{Data}) d\boldsymbol{\nu}_{j,\alpha}(\boldsymbol{\theta}) = \frac{1}{\alpha} \int h(\boldsymbol{\nu}_{j,\alpha}(\boldsymbol{\theta}))f(\boldsymbol{\theta}|\text{Data})d\boldsymbol{\theta}, \quad (10)$$

which allows us to run MCMC with the original posterior as the target, map the drawn $\boldsymbol{\theta}$ to $\boldsymbol{\nu}_{j,\alpha}(\boldsymbol{\theta})$, and compute $h(\boldsymbol{\nu}_{j,\alpha})$ for eventual summarization and estimation.

Given the samples $\{\boldsymbol{\theta}^{(b)} : b = 1, \dots, B\}$ directly drawn from the posterior distribution $f(\boldsymbol{\theta}|\mathbf{y})$ using MCMC, define $\boldsymbol{\nu}_{j,\alpha}^{(b)} = \left(\theta_1^{(b)}, \dots, \theta_{j-1}^{(b)}, \alpha\theta_j^{(b)}, \theta_{j+1}^{(b)}, \dots, \theta_p^{(b)}\right)$ with a pre-specified set of α (near 1) under the intervention posterior. A full suite of inferences is available through $h(\boldsymbol{\nu}_{j,\alpha}^{(b)})$ for each j , with varying values of α . One straightforward way to estimate (10) is to use $(1/B) \sum_{b=1}^B h(\boldsymbol{\nu}_{j,\alpha}^{(b)})$ with which we can assess the average change of the outcome $h(\cdot)$ as we decrease or increase the j th parameter by $100(1-\alpha)\%$. Other inferences, such as variances, quantiles, or credible intervals, can be obtained similarly.

The intervention posterior is closely related to the importance link function transformation of MacEachern and Peruggia (2000). Their key assumption is that estimated parameters are drawn from a sampling distribution that is different from a target distribution, and a known link function is used to map the sampled values from the sampling distribution to those of the target distribution. In our intervention posterior framework, the closed form of a link function is not available, yet the ODE model operates as the importance link function, mapping the posterior sample space to the intervention sample space.

The discussion of the intervention posterior so far assumes that the posterior samples are drawn from standard Metropolis-Hastings. When a generalized multiset sampler is used, the summary under the intervention posterior can be computed as $(1/B) \sum_{b=1}^B \sum_{m=1}^M w_m^{(b)} h(\boldsymbol{\nu}_{m,j,\alpha}^{(b)})$ where $h(\boldsymbol{\nu}_{m,j,\alpha}^{(b)})$ is obtained by running the ODE model with the j -th variable of $\boldsymbol{\theta}_m^{(b)}$ of the m th multiset element scaled by α .

5 Calibration of a Three-variable Biochemical Oscillator

In this section, we present our proposed calibration approach applied to the physical and computer experiments for the circadian cycle of *Neurospora crassa*. There are several critical challenges that need to be addressed in this application, each of which will be described in a subsection.

5.1 Application of the GMSS

To apply GMSS, it is important to have a set of working instrumental densities as discussed in Section 3.2. To this end, we conducted prognostic experiments as described in Section 3.3, where 100 independent batches of randomized orthogonal array designs based on a full 3^9 factorial design were conducted. This took 17 hours using 36 Xeon E5-2680 cores. Since each batch could be executed without coordination between the computing nodes, the job could be readily distributed over many cores, taking advantage of the parallel computing resources. The sub-dimension used in the search process was $d_0 = 4$, with $n_{\min} = 0$. A minimum log-likelihood $l_{\min} = -150$ was used, corresponding approximately to the 0.1% percentile of the evaluations. That is, any experiments with log-likelihood higher than -150

were deemed successful, and any level combination in the 3^9 design that matches in four columns or more with a single successful run were given $\rho_1 = 1.0$, and $\rho_0 = 0.1$ otherwise. Hence, the Markov chain was ten times more likely to search the area with successful prognostic runs than that with unsuccessful runs. Instrumental densities gave $\rho_1 = 1.0$ to 13% (2,585/19,683) of the level combinations in 3^9 factorial designs.

With the obtained instrumental densities, the GMSS finds a wide range of areas whose likelihood functions have high values. Figure 3 shows the trace of the multiset component whose weight w_m is the largest among the $M = 20$ components at each iterate b . The leading component with the highest weight frequently switches from one to another, showing that each component of the GMSS finds high density regions spread around the whole parameter space. The trace plots also suggest that many regions have similar likelihood values, while the high density regions are often distant from each other with wide low density regions between them in the multi-dimensional space as shown in Figure A1 of Appendix.

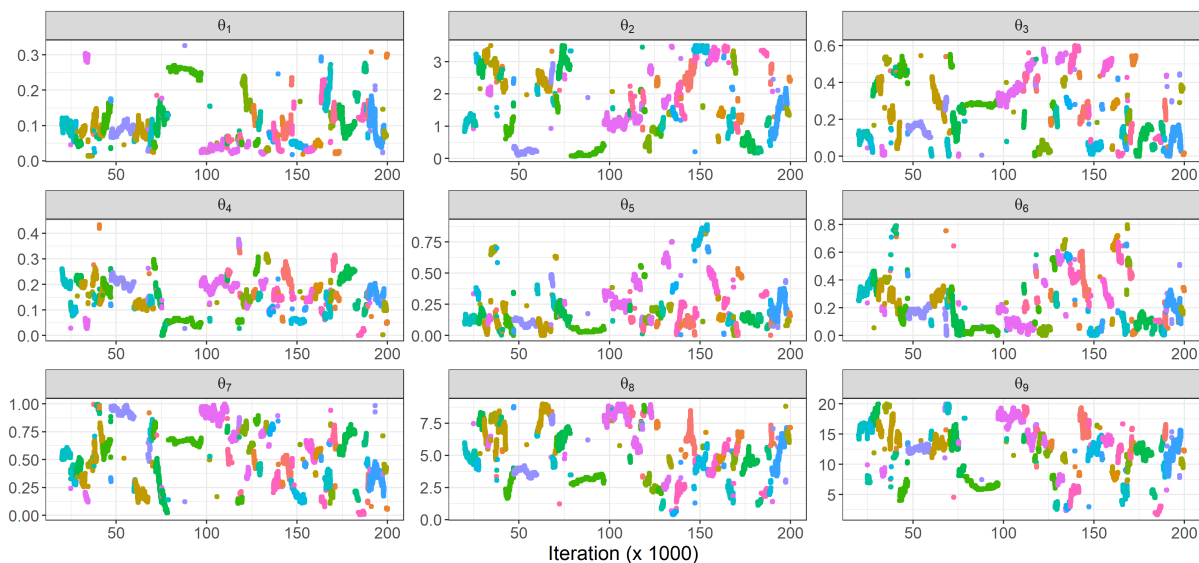


Figure 3: Trace plots of the multiset component with largest weight w_m among $M = 20$ components, where color coding indicates different components.

Figure 4 presents the cumulative histogram of the summarized MCMC samples as of

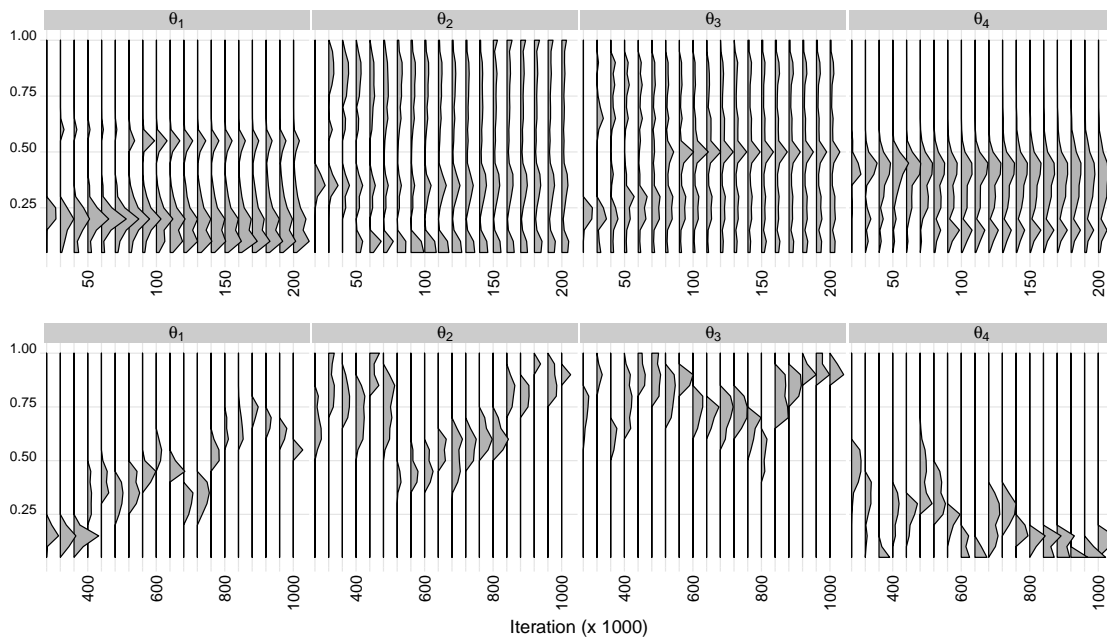


Figure 4: Cumulative histogram of posterior samples of four parameters from GMSS (top) and Metropolis-Hastings as of each iteration (bottom), where all parameter ranges are scaled to $(0, 1]$.

the latest iteration for the first four variables, comparing the results from GMSS and Metropolis-Hastings samples. With the GMSS, the chain successfully converged and mixed well in 200,000 iterations. Its Markov chain reaches the stationary distribution after about 130,000 iterations as the cumulative histogram does not change its shape after this point. On the contrary, an ordinary Metropolis-Hastings chain failed to reach a stationary distribution even after 1 million iterations. The cumulative histogram from Metropolis-Hastings samples keeps changing its shape as more samples accrue, which suggests that the sampling failed to converge to a stationary distribution.

5.2 Sensitivity Analysis with Intervention Posterior

We conduct a sensitivity analysis using the intervention posterior defined in (9) with GMSS samples. The scientific contribution of our approach is to allow an extensive parameter calibration along with its uncertainty quantification, which is summarized in Figure 5.

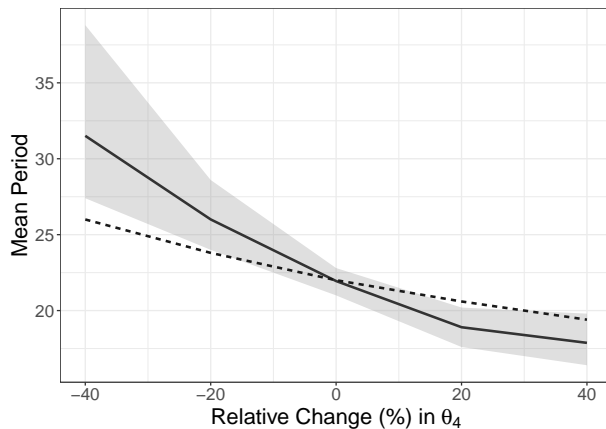


Figure 5: The intervention posterior results are shown in the solid line with 80% credible interval. The sensitivity analysis from Caicedo-Casso et al. (2015) is overlaid in the dashed line.

Caicedo-Casso et al. (2015) manually explore the parameter space of the ODE to find a single parameter value to represent the system. Once established, the impact of intervention is explored by changing the value of θ_4 while holding other parameters fixed and then examining the change in the circadian cycle as a function of the varying θ_4 value. In contrast, our approach relies on the intervention posterior to examine the sensitivity of the circadian cycle to changes in θ_4 . Since the posterior distribution shows considerable dispersion and our inferential target is a very nonlinear function of the parameters, we might expect to find differences between sensitivity in the single parameter approach and the intervention posterior approach. We do find differences. To illustrate this, we superimpose the result from Caicedo-Casso et al. (2015) over our results in Figure 5. Both approaches show an overall trend where a low value of θ_4 is associated with a higher frequency for the circadian cycle. However, Caicedo-Casso et al. (2015) underestimates the sensitivity as their single estimate lies, for the most part, outside of the 80% credible interval.

The differences between the two approaches stem from the treatment of the parameters other than θ_4 . The physical experiment provides limited information about the system's parameters. In such a situation, selecting a single parameter value about which to consider

perturbations misses the fact that the impact of perturbation could be very different for other parameter values. In this setting, our inferential target (duration of the circadian cycle) is a highly nonlinear function of the parameters, and so the sensitivity to perturbation of a baseline parameter value varies considerably. The intervention posterior allows us to capture this variation and to provide summaries to the biologist that encapsulate our knowledge – and our lack of knowledge – of the system. In addition to providing a different curve for mean sensitivity, the intervention posterior provides a distribution on sensitivity to change in θ_4 for each given value of α .

Figure 6 shows the posterior sensitivity for duration of the circadian cycle, evaluated with $\alpha = (0.6, 0.8, 1.0, 1.2, 1.4)$. The points and lines indicate the mean circadian cycle while the shaded areas represent the 80% credible intervals. The strong slope in the plot for θ_4 shows that this parameter affects periodicity the most. The parameters θ_2 , θ_3 , and perhaps θ_6 , seem inert, whereas θ_1 , θ_5 , and θ_7 show a modest effect on period. The parameters θ_8 and θ_9 show a moderate effect on period through the mean, yet the striking feature for these parameters is the great width of the credible intervals. This indicates that the effect on period varies substantially, depending on the values of the other parameters in the system. In other words, these parameters show evidence of a substantial interaction for the response of period.

Figure 7 shows a heat map for posterior mean period, considering perturbation of two parameters at a time. Each of the parameters is perturbed with α ranging from 0.6 to 1.4. The size of the perturbation is given on the axes of the figure. The plotted (heat) value is the relative change in period. These plots are effective in conveying the sensitivity of period to perturbation and in conveying interactions or the lack thereof. For instance, consider θ_2 . The upper left plot, for (θ_1, θ_2) , shows essentially no variation in the vertical direction.

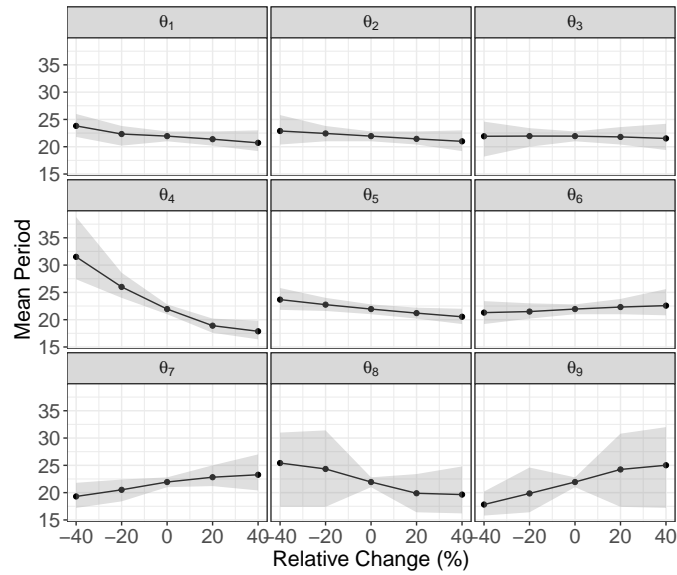


Figure 6: Sensitivity analysis of all nine variables using the intervention posterior approach, where the dots and line indicates the posterior mean, and the shaded area represents the 80% credible interval.

This tells us that changing the value of θ_2 has essentially no impact on period and that there is no $\theta_1 \times \theta_2$ interaction. Similarly, the lack of variation in the horizontal direction for plots in the second column shows that θ_2 has no appreciable interaction with any of the other parameters in the model (when the response is period). Turning to θ_8 and θ_9 , the diagonal stripe in the lower right-hand plot shows a strong interaction between the two parameters. Period is increased by reducing θ_8 and increasing θ_9 . The reverse perturbation, increasing θ_8 and reducing θ_9 is forecast to have little effect on period. The intensity of color for θ_4 shows its impact on period. The patterns in the plots show the importance of other parameters' interaction with θ_4 . In particular, perturbation of θ_1 (lower values), θ_8 (lower values) and θ_9 (higher values) suggest longer periods.

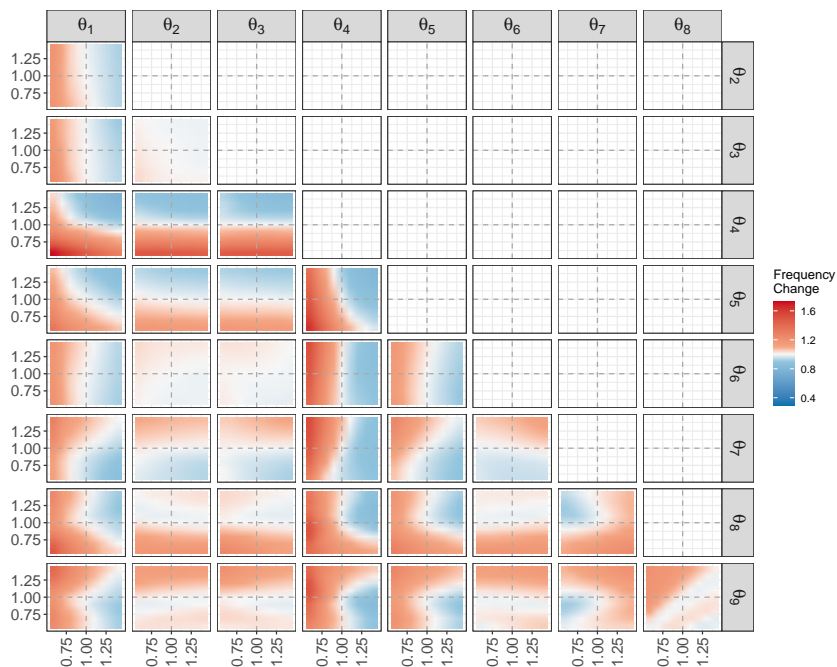


Figure 7: Sensitivity analysis of all pairs of variables using the intervention posterior approach, where color represents the relative change in main frequency.

6 Discussion

In this work, we address a challenging scientific problem in analyzing oscillatory phenomena in biological systems. The proposed framework provides a rigorous methodology for model calibration, uncertainty quantification, and sensitivity analysis for biological studies investigating periodic phenotypes. The generalized multiset sampler, equipped with instrumental densities obtained from prognostic experiments, successfully finds posterior densities that lie in a very thin high-dimensional manifold. The intervention posterior approach is devised for an intuitive yet rigorous sensitivity analysis to better utilize the result from Bayesian calibration. Our case study presents an overhaul of the analysis of the model from Caicedo-Casso et al. (2015). Placing the analysis in a statistical framework generates more insights. It is expected that our method will attract wide research interest from biology communities studying oscillatory phenomena ranging from cell cycle to circadian rhythms.

We conclude with remarks on potential future research topics. First, the intervention posterior is a useful tool for sensitivity analysis, providing access to counterfactual scenarios through the biological computer models. It is closely related to the concept of expected effect size; hence sample size calculation can be an immediate research topic to follow. Second, we consider a fully deterministic model based on differential equations. When studying a long series of data, a model with a stochastic evolution of the system can be more useful because the governing system itself can evolve over time. Such models can shed light on the relationship between model and parameter complexity. A stochastic model with fewer yet time-varying parameters can be comparable to a deterministic model with many fixed parameters. Calibrating such stochastic models poses some unique challenges and requires development of a new calibration approach (e.g., Chkrebtii et al., 2016). The intervention posterior may need a suitable modification for those cases.

Appendix: The appendix presents detailed steps for an ordinary Metropolis-Hastings algorithm for the considered model, as well as some additional quantitative information for the analysis in the case study.

References

- Aronson, B. D., Johnson, K. A., Loros, J. J., and Dunlap, J. C. (1994), “Negative feedback defining a circadian clock: autoregulation of the clock gene frequency,” *Science*, 263, 1578–1584.
- Bayarri, M., Berger, J., Cafeo, J., Garcia-Donato, G., Liu, F., Palomo, J., Parthasarathy, R., Paulo, R., Sacks, J., Walsh, D., et al. (2007), “Computer model validation with functional output,” *Annals of Statistics*, 35, 1874–1906.

- Bellman, J., Kim, J. K., Lim, S., and Hong, C. I. (2018), “Modeling reveals a key mechanism for light-dependent phase shifts of neurospora circadian rhythms,” *Biophysical Journal*, 115, 1093–1102.
- Bellprat, O., Kotlarski, S., Lüthi, D., and Schär, C. (2012), “Objective calibration of regional climate models,” *Journal of Geophysical Research: Atmospheres*, 117.
- Bhat, K., Haran, M., Olson, R., and Keller, K. (2012), “Inferring likelihoods and climate system characteristics from climate models and multiple tracers,” *Environmetrics*, 23, 345–362.
- Caicedo-Casso, A., Kang, H.-W., Lim, S., and Hong, C. I. (2015), “Robustness and period sensitivity analysis of minimal models for biochemical oscillators,” *Scientific Reports*, 5, 1–15.
- Chang, K.-L. and Guillas, S. (2019), “Computer model calibration with large non-stationary spatial outputs: application to the calibration of a climate model,” *Journal of the Royal Statistical Society: Series C (Applied Statistics)*, 68, 51–78.
- Chang, W., Haran, M., Applegate, P., and Pollard, D. (2016), “Calibrating an ice sheet model using high-dimensional binary spatial data,” *Journal of American Statistical Association*, 111, 57–72.
- Chang, W., Haran, M., Olson, R., Keller, K., et al. (2014), “Fast dimension-reduced climate model calibration and the effect of data aggregation,” *Annals of Applied Statistics*, 8, 649–673.
- Chkrebtii, O. A., Campbell, D. A., Calderhead, B., and Girolami, M. A. (2016), “Bayesian

- solution uncertainty quantification for differential equations,” *Bayesian Analysis*, 11, 1239–1267.
- Cox, K. H. and Takahashi, J. S. (2019), “Circadian clock genes and the transcriptional architecture of the clock mechanism,” *Journal of Molecular Endocrinology*, 63, R93–R102.
- Dunlap, J. C. and Loros, J. J. (2017), “Making time: conservation of biological clocks from fungi to animals,” *Microbiology Spectrum*, 5, 5–3.
- Gallego, M., Eide, E. J., Woolf, M. F., Virshup, D. M., and Forger, D. B. (2006), “An opposite role for tau in circadian rhythms revealed by mathematical modeling,” *Proceedings of the National Academy of Sciences*, 103, 10618–10623.
- Geoghegan, R. (2006), *Time Series Analysis and Its Applications: with R Examples*, New York: Springer.
- Geyer, C. J. (1991), “Markov chain Monte Carlo maximum likelihood,” in *Computing Science and Statistics: Proceedings of the 23rd Symposium on the Interface*, ed. Keramides, E. M., Fairfax Station, Va.: Interface Foundation, pp. 156–163.
- Gooch, V. D., Johnson, A. E., Bourne, B. J., Nix, B. T., Maas, J. A., Fox, J. A., Loros, J. J., Larrondo, L. F., and Dunlap, J. C. (2014), “A kinetic study of the effects of light on circadian rhythmicity of the *frq* promoter of *Neurospora crassa*,” *Journal of Biological Rhythms*, 29, 38–48.
- Goodfellow, M., Phillips, N. E., Manning, C., Galla, T., and Papalopulu, N. (2014), “MicroRNA input into a neural ultradian oscillator controls emergence and timing of alternative cell states,” *Nature Communications*, 5, 1–10.

- Gotoh, T., Kim, J. K., Liu, J., Vila-Caballer, M., Stauffer, P. E., Tyson, J. J., and Finkielstein, C. V. (2016), “Model-driven experimental approach reveals the complex regulatory distribution of p53 by the circadian factor Period 2,” *Proceedings of the National Academy of Sciences*, 113, 13516–13521.
- Gramacy, R. B., Bingham, D., Holloway, J. P., Grosskopf, M. J., Kuranz, C. C., Rutter, E., Trantham, M., Drake, R. P., et al. (2015), “Calibrating a large computer experiment simulating radiative shock hydrodynamics,” *Annals of Applied Statistics*, 9, 1141–1168.
- Hartley, H. O. (1949), “Tests of significance in harmonic analysis,” *Biometrika*, 36, 194–201.
- Higdon, D., Gattiker, J., Williams, B., and Rightley, M. (2008), “Computer model calibration using high-dimensional output,” *Journal of the American Statistical Association*, 103, 570–583.
- Hwang, Y., Barut, E., and Yeo, K. (2018), “Statistical-physical estimation of pollution emission,” *Statistica Sinica*, 921–940.
- Karagiannis, G. and Lin, G. (2017), “On the Bayesian calibration of computer model mixtures through experimental data, and the design of predictive models,” *Journal of Computational Physics*, 342, 139–160.
- Kennedy, M. C. and O’Hagan, A. (2001), “Bayesian calibration of computer models,” *Journal of the Royal Statistical Society: Series B (Statistical Methodology)*, 63, 425–464.
- Kim, H. J. and MacEachern, S. N. (2015), “The generalized multiset sampler,” *Journal of Computational and Graphical Statistics*, 24, 1134–1154.
- Kirkpatrick, S. (1984), “Optimization by simulated annealing: Quantitative studies,” *Journal of Statistical Physics*, 34, 975–986.

- Lee, B. S., Haran, M., Fuller, R. W., Pollard, D., Keller, K., et al. (2020), “A fast particle-based approach for calibrating a 3-D model of the Antarctic ice sheet,” *Annals of Applied Statistics*, 14, 605–634.
- Leman, S. C., Chen, Y., and Lavine, M. (2009), “The multiset sampler,” *Journal of the American Statistical Association*, 104, 1029–1041.
- Liu, J. S., Liang, F., and Wong, W. H. (2000), “The multiple-try method and local optimization in Metropolis sampling,” *Journal of the American Statistical Association*, 95, 121–134.
- Liu, X., Chen, A., Caicedo-Casso, A., Cui, G., Du, M., He, Q., Lim, S., Kim, H. J., Hong, C. I., and Liu, Y. (2019), “FRQ-CK1 interaction determines the period of circadian rhythms in *Neurospora*,” *Nature Communications*, 10, 1–13.
- MacEachern, S. N. and Peruggia, M. (2000), “Importance link function estimation for Markov chain Monte Carlo methods,” *Journal of Computational and Graphical Statistics*, 9, 99–121.
- Mak, S., Sung, C.-L., Wang, X., Yeh, S.-T., Chang, Y.-H., Joseph, V. R., Yang, V., and Wu, C. J. (2018), “An efficient surrogate model for emulation and physics extraction of large eddy simulations,” *Journal of the American Statistical Association*, 113, 1443–1456.
- Marinari, E. and Parisi, G. (1992), “Simulated tempering: a new Monte Carlo scheme,” *EPL (Europhysics Letters)*, 19, 451.
- Oguz, C., Laomettachit, T., Chen, K. C., Watson, L. T., Baumann, W. T., and Tyson, J. J. (2013), “Optimization and model reduction in the high dimensional parameter space of a budding yeast cell cycle model,” *BMC Systems Biology*, 7, 1–17.

- Peifer, M. and Timmer, J. (2007), “Parameter estimation in ordinary differential equations for biochemical processes using the method of multiple shooting,” *IET Systems Biology*, 1, 78–88.
- Sassone-Corsi, P., Young, M. W., and Reddy, A. B. (2018), *Circadian rhythms: a subject collection from Cold Spring Harbor perspectives in biology*, Cold Spring Harbor New York: Cold Spring Harbor Laboratory Press.
- Sha, W., Moore, J., Chen, K., Lassaletta, A. D., Yi, C.-S., Tyson, J. J., and Sible, J. C. (2003), “Hysteresis drives cell-cycle transitions in *Xenopus laevis* egg extracts,” *Proceedings of the National Academy of Sciences*, 100, 975–980.
- Storn, R. and Price, K. (1997), “Differential evolution—a simple and efficient heuristic for global optimization over continuous spaces,” *Journal of Global Optimization*, 11, 341–359.
- Sung, C.-L., Hung, Y., Rittase, W., Zhu, C., and Wu, C. F. J. (2020), “Calibration for computer experiments with binary responses and application to cell adhesion study,” *Journal of the American Statistical Association*, 115, 1664–1674.
- Swendsen, R. H. and Wang, J.-S. (1986), “Replica Monte Carlo simulation of spin-glasses,” *Physical Review Letters*, 57, 2607.
- Tang, B. (1993), “Orthogonal array-based Latin hypercubes,” *Journal of the American Statistical Association*, 88, 1392–1397.
- Tsai, T. Y.-C., Choi, Y. S., Ma, W., Pomerening, J. R., Tang, C., and Ferrell, J. E. (2008), “Robust, tunable biological oscillations from interlinked positive and negative feedback loops,” *Science*, 321, 126–129.

- Tu, B. P., Kudlicki, A., Rowicka, M., and McKnight, S. L. (2005), “Logic of the yeast metabolic cycle: temporal compartmentalization of cellular processes,” *Science*, 310, 1152–1158.
- Tuo, R., Wu, C. J., et al. (2015), “Efficient calibration for imperfect computer models,” *Annals of Statistics*, 43, 2331–2352.
- Williams, B., Christensen, W. F., and Reese, C. S. (2011), “Pollution source direction identification: embedding dispersion models to solve an inverse problem,” *Environmetrics*, 22, 962–974.
- Wu, C. J. and Hamada, M. S. (2011), *Experiments: Planning, Analysis, and Optimization*, New Jersey: John Wiley & Sons.

A Appendix

A.1 (Standard) Metropolis-within-Gibbs for Model (6)

1. For each $j = 1, \dots, p(= 19)$, update the ODE model parameter θ_j (i.e., $\boldsymbol{\lambda}$ by Metropolis-Hastings with the normal proposal density $g(\theta_j^q | \theta_j) \sim N(\theta_j, \text{stepsize}^2)$ and the acceptance probability $\min(1, a)$ where

$$a = \frac{\left[\prod_{i=1}^n \prod_{k=1}^K f(s_{ik} | \lambda_k(\boldsymbol{\theta}^q), \tau^2) \right] f(\boldsymbol{\theta}^q)}{\left[\prod_{i=1}^n \prod_{k=1}^K f(s_{ik} | \lambda_k(\boldsymbol{\theta}), \tau^2) \right] f(\boldsymbol{\theta})}$$

where $\lambda_k(\boldsymbol{\theta}^q)$ is computed by ODE and spectral analysis for the proposed ODE parameter $\boldsymbol{\theta}^q = (\theta_1, \dots, \theta_{j-1}, \theta_j^q, \theta_{j+1}, \dots, \theta_p)$.

2. For each $i = 1, \dots, n(= 3)$, update \mathbf{s}_i by Metropolis-Hastings with the normal proposal density $g(\mathbf{s}_i^q | \mathbf{s}_i) \sim N(\mathbf{s}_i, \text{stepsize}^2 \mathbf{I})$ and the acceptance probability $\min(1, a)$ where

$$a = \frac{f(\widehat{\mathbf{S}}_i | \mathbf{s}_i^q) f(\mathbf{s}_i^q | \boldsymbol{\lambda}, \tau^2)}{f(\widehat{\mathbf{S}}_i | \mathbf{s}_i) f(\mathbf{s}_i | \boldsymbol{\lambda}, \tau^2)}.$$

3. Update τ^2 with $g(\tau^{2q} | \tau^2) \sim N(\tau^2, \text{stepsize}^2)$ and the acceptance probability $\min(1, a)$ where

$$a = \frac{\left[\prod_{i=1}^n \prod_{k=1}^K f(s_{ik} | \lambda_k(\boldsymbol{\theta}^q), \tau^{2q}) \right] f(\tau^{2q})}{\left[\prod_{i=1}^n \prod_{k=1}^K f(s_{ik} | \lambda_k(\boldsymbol{\theta}), \tau^2) \right] f(\tau^2)}.$$

4. Update σ^2 by Metropolis-Hastings with the normal proposal density $g(\sigma^{2q} | \sigma^2) \sim N(\sigma^2, \text{stepsize}^2)$ and the acceptance probability $\min(1, a)$ where

$$a = \frac{\left[\prod_{i=1}^n \prod_{k=1}^K f(s_{ik} | \lambda_k, \tau^2, \sigma^{2q}) \right] f(\sigma^{2q})}{\left[\prod_{i=1}^n \prod_{k=1}^K f(s_{ik} | \lambda_k, \tau^2, \sigma^2) \right] f(\sigma^2)}.$$

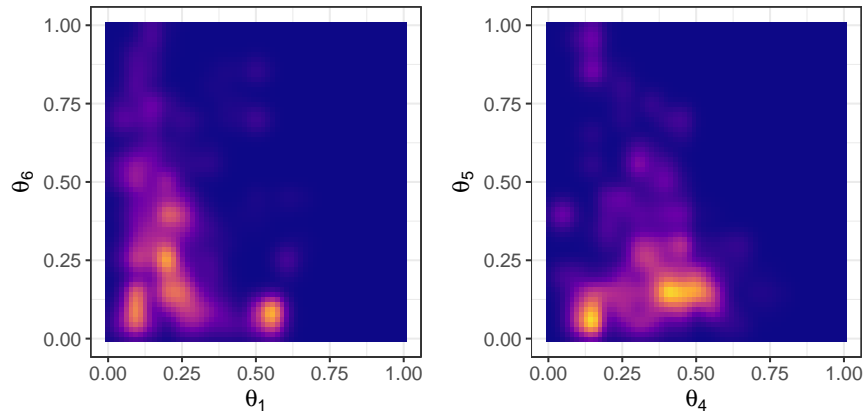


Figure A1: Bivariate posterior distribution of (θ_1, θ_6) and (θ_4, θ_5) obtained from GMSS

A.2 Some Additional Results

In this section, we provide some additional analysis results to better present our overall approach.

Figure A1 presents a pair of heatmaps of bivariate posterior distribution. Standard Metropolis-Hastings is hindered by the complexity of the distribution, while GMSS successfully converges to the target distribution.

Figures 6 and 7 in the manuscript have focused on graphical summary from the intervention posterior, yet (10) is applicable for various situations. If the experimenter is more interested in posterior probabilities with quantitative information, Table A1 provides this information in depth. For example, when θ_4 is scaled down to 60% of its current values, circadian cycle period is almost certainly increased 10% from that of experimental data. As biologists are more interested in the increase in the circadian cycle than decrease, we only present the cases for increased cycles. The intervention posterior also provides an analysis to find the boundary of oscillating regions enveloping the current parameters, called *bifurcation* analysis (Caicedo-Casso et al., 2015; Liu et al., 2019). Such results are summarized as the proportion of runs that fail to converge, corresponding to the amount of change in parameter values.

	α	Failure	Period + 10%	Period + 20%	Period + 30%	Period + 40%
θ_1	0.6	0.00	100.00	11.57	0.00	0.00
	0.8	0.00	0.00	0.00	0.00	0.00
	1.2	0.00	0.00	0.00	0.00	0.00
	1.4	0.00	0.00	0.00	0.00	0.00
θ_2	0.6	0.00	18.53	7.80	0.00	0.00
	0.8	0.00	4.88	0.00	0.00	0.00
	1.2	0.00	0.00	0.00	0.00	0.00
	1.4	0.00	0.00	0.00	0.00	0.00
θ_3	0.6	0.00	13.15	0.19	0.00	0.00
	0.8	0.00	0.19	0.00	0.00	0.00
	1.2	0.00	5.70	0.00	0.00	0.00
	1.4	0.00	9.29	4.27	0.00	0.00
θ_4	0.6	0.00	100.00	97.78	77.82	35.30
	0.8	0.00	97.78	30.45	2.27	0.16
	1.2	0.00	0.00	0.00	0.00	0.00
	1.4	16.10	0.00	0.00	0.00	0.00
θ_5	0.6	0.00	37.46	1.29	0.16	0.00
	0.8	0.00	0.27	0.00	0.00	0.00
	1.2	0.00	0.00	0.00	0.00	0.00
	1.4	0.00	0.00	0.00	0.00	0.00
θ_6	0.6	0.00	4.11	0.00	0.00	0.00
	0.8	0.00	0.00	0.00	0.00	0.00
	1.2	0.00	9.75	0.00	0.00	0.00
	1.4	0.00	16.58	7.71	0.00	0.00
θ_7	0.6	9.44	1.48	0.00	0.00	0.00
	0.8	0.00	0.00	0.00	0.00	0.00
	1.2	0.00	15.30	0.48	0.00	0.00
	1.4	0.00	32.21	12.15	0.87	0.16
θ_8	0.6	41.52	68.10	53.28	31.88	14.29
	0.8	7.09	53.50	36.42	16.36	12.38
	1.2	23.82	7.69	0.00	0.00	0.00
	1.4	62.06	12.05	1.23	0.00	0.00
θ_9	0.6	87.65	0.00	0.00	0.00	0.00
	0.8	48.05	11.68	0.90	0.00	0.00
	1.2	6.61	53.82	33.95	15.72	11.36
	1.4	23.62	59.34	48.42	26.91	16.20

Table A1: Additional summary of posterior probabilities, where columns on the right show the proportions of experiments that failed to converge (Failure), and the experiments that led to an increase in circadian cycle periods exceeding certain percentage range.